Steady State α→γ-Recrystallization of Ferritic Iron Alloys with a Cellular Structure of the Interfacial Surface during Carburization

K. O. Chornoivanenko and O. V. Movchan

Ukrainian State University of Science and Technologies,
2 Lazariana Str.,
UA-49010 Dnipro, Ukraine

The mathematical model of single-phase cellular growth of the γ-phase layer during isothermal α→γ-recrystallization of a carburized ferritic iron alloy is constructed based on the performed analysis. Diffusion transfer of carbon through the γ-phase to the interphase surface is the main factor that determines the kinetics of α→γ-recrystallization during carburization. The expression for the distribution of carbon within the γ-phase in front of the flat phase interface (PI) during a steady-state process is obtained. The near-boundary concentration differences between the curved and flat PI are determined. The near-boundary mole fractions of the components inside the α- and γ-phases are calculated. Diffusion processes within the α-phase before PI are described. The expression relating diffusion processes within the α-phase in front of PI with the velocity of front advancement is obtained. Longitudinal sections of cells corresponding to limiting cases of surface-tension coefficient σ and microstructures during α→γ-recrystallization are presented. As shown, the PI cells have a pronounced crystalline facet during solid-phase recrystallization. In this case, the morphology of the cells depends on the crystallographic direction of growth of the γ-phase.

Key words: recrystallization, phase interface, cellular growth, carburization, stationary process, *in situ* composite.

Corresponding author: Kateryna Oleksandrivna Chornoivanenko
E-mail: ekatmovchan@gmail.ua

Проведено аналізу й на підставі неї побудовано математичний модель однофазного коміркового зростання шару γ-фази під час ізотермічної α→γ-перекристалізації феритного стопу заліза за навуглецьовування. Встановлено, що основним чинником, що визначає кінетику α→γ-перекристалізації за навуглецювання, є дифузійна доставляння Карбону через γ-фазу до міжфазної поверхні. Було одержано вираз для розподілу Карбону в γ-фазі перед пласкою фазовою поверхнею за стаціонарного процесу. Визначено ріжниці примежових концентрацій між викривленою та пласкою фазовою поверхнею. Було розраховано примежові мольні частки компонентів у α- й γ-фазах. Описано дифузійні процеси у α-фазі перед фазовою поверхнею. Одержано вираз, що зв'язує дифузійні процеси у α-фазі перед фазовою поверхнею зі швидкістю просування фронту. Представлено поздовжні перерізи комірок, що відповідають граничним випадкам значень коефіцієнта поверхневого натягу σ та мікроструктурам під час α→γ-перекристалізації. Показано, що комірки фазової поверхні мають виражене кристалічне огранування за твердофазної перекристалізації. Воднораз морфологія комірок залежить від кристалографічного напрямку зростання γ-фази.

Ключові слова: перекристалізація, фронт перетворення, коміркове зростання, навуглецьовування, стаціонарний процес, *in situ*-композит.

1. INTRODUCTION

The development of diffusion structures in multiphase, multicomponent alloys presents many features of metallurgical interest for study [1]. One of these features is the morphology of interfaces between diffusion layers. Interfaces can be planar or non-planar and affect not only the growth of layers but also the evolution of diffusion structure.

The paper [2] analysed theoretical information about morphological stability of the transformation front during phase reactions. The theory of concentration supercooling is considered, the basis of which is diffusion redistribution of alloy components in a melt near crystallization boundary. The authors [3–8] have established that the cellular structure of the interphase boundary arises in the case when the interphase surface becomes unstable to wave distortions. It is also found that transformation of a conversion front is carried out under the action of concentration gradients.

Many researchers consider that the main reason for front curvature and appearance of periodic structures is instability of the interphase boundary in the process of phase transition. There are many theoretical calculations that give qualitative correspondences of one or another mathematical model of directional crystallization with observable structures since the classical paper [3].

The authors of Refs. [9, 10] observed the phenomenon of flat front

transformation into cellular front at α→γ-recrystallization of carburized Fe−Si alloys. The effect of concentration supersaturation of ferrite by carbon explained that. It was analogous to concentration supercooling during crystallization of alloys.

Many articles related to phase and structural transformations of ferritic Fe−*Me* alloys during carburization have been published to date [11−20]. Some of these articles [18−20] show that under certain conditions of the carburization process, the flat front of the α→γ-polymorphic transformation (PI—phase interface) becomes unstable. It transforms first into cellular PI (Fig. 1, *a*, *b*), and then into dendritic PI (Fig. 1, *c*). The stability of the planar PI was analysed using the well-known perturbation method of Mullins and Sekerka [3]. The results generally correspond to the results obtained by studying the crystalli-
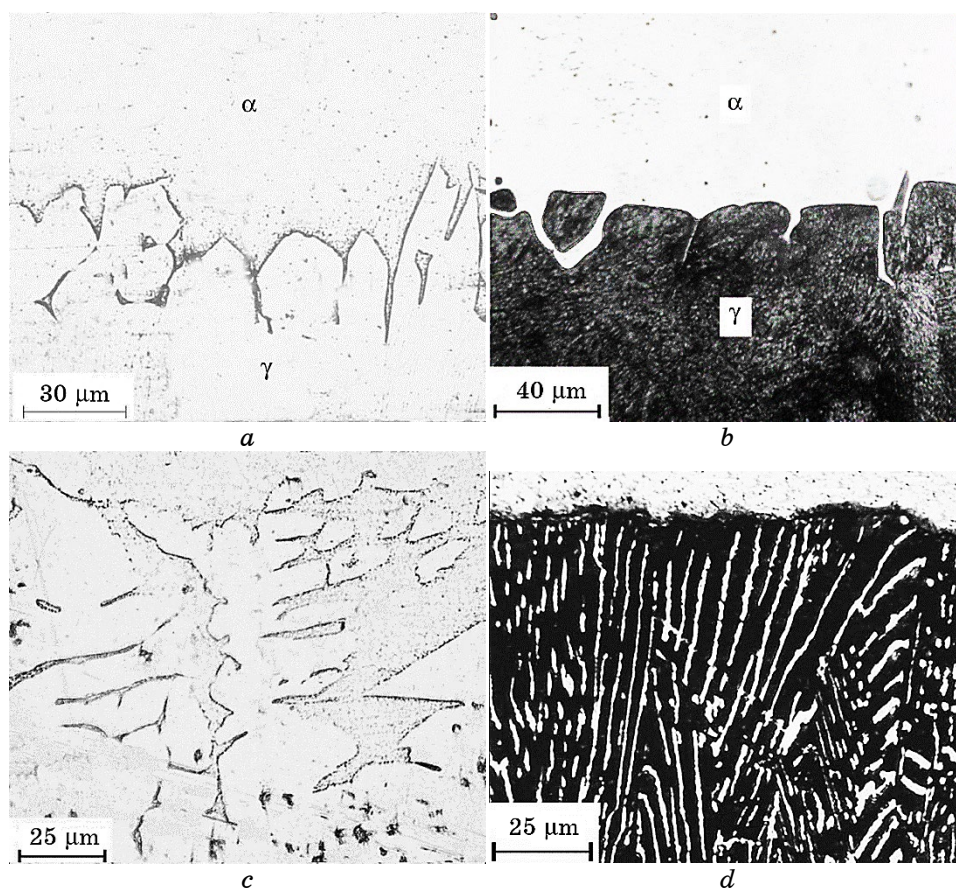
Fig. 1. Structure of the PI of Fe−25% Cr−0.027% Si alloy during carburization.

zation of various alloys. The most significant factors affecting the stability of a flat front are the speed of its advance, the concentration (mole fraction) of the α-stabilizer, as well as the difference between the equilibrium concentrations of components in ferrite and austenite [20].

Carburization of iron alloys with a carbide-forming α-stabilizer makes it possible to obtain materials with *in situ* composite structure in the surface layer. The composite is an austenitic (martensitic) matrix reinforced with fibres or plates of special carbides (Fig. 1, *d*). The plates or fibres are oriented along the carbon flow. This structure of the carburized layer corresponds to a special set of performance properties, in particular, high wear resistance. Violation of the unidirectionality of the reinforcing carbide phase due to the development of a cellular structure leads to a decrease or loss of the required characteristics.

The aim of this work is to analyse and construct a mathematical model of single-phase cellular growth of a γ-phase layer of a carburized ferritic iron alloy during isothermal $\alpha{\to}\gamma$-recrystallization.

2. THEORETICAL DETAILS

2.1. Research of Concentration on the PI

The following assumptions were made for subsequent calculations: 1) the mole fractions of components at the interphase boundaries correspond to the equality of the chemical potentials of these components (taking into account the curvature of the boundaries); 2) the mole fraction of carbon in the initial α-phase corresponds to its maximum solubility at a given temperature and the mole fraction of the α-stabilizer. This is observed in most real systems; 3) the space in front of PI was considered semi-infinite.

The isothermal section of the Fe$-Me-$C phase diagram was used to calculate near-surface concentrations (where *Me* is an α-stabilizer). In Figure 2, it is shown a diagram of a section of the Fe$-Me-$C phase diagram at a temperature above the temperature of $\alpha-\gamma$-iron polymorphism. The following designations are accepted: $^{\min}X_k^{f_1/f_2}$ is minimum mole fraction of component k in phase f_1 at the interface boundary with phase f_2, $^{\max}X_k^{f_1/f_2}$ is maximum mole fraction of component k in phase f_1 at the interface boundary with phase f_2, $^{p}X_k^{f_1/f_2}$ is mole fraction of component k in phase f_1 on flat PI; $^{\infty}X_k^{f}$ is mole fraction of component k in the f-phase at an infinite distance from PI.

The fractions of components on both sides of the interface boundary can be determined from the phase diagram using a simple relationship with a known value of the mole fraction of one of their components (*e.g.*, $X_k^{f_1/f_2}$):
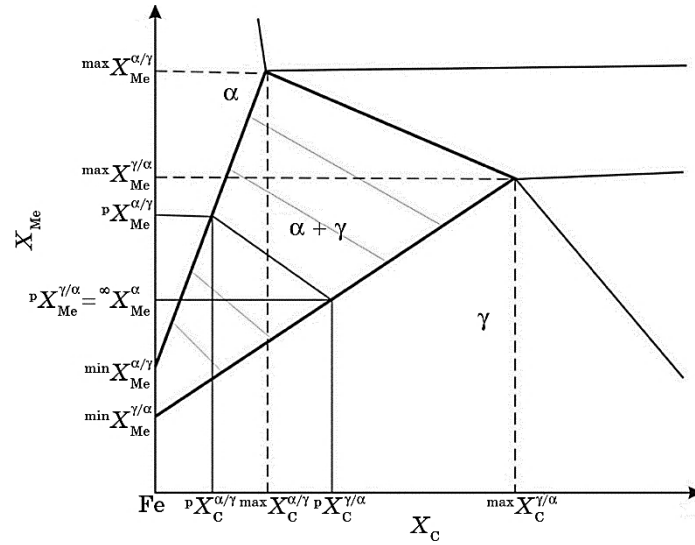
Fig. 2. Scheme of the isothermal section of the Fe−*Me*−C phase diagram.

$$K = \frac{X_{k_1}^{f_1/f_2} - {}^{\min}X_{k_1}^{f_1/f_2}}{{}^{\max}X_{k_1}^{f_1/f_2} - {}^{\min}X_{k_1}^{f_1/f_2}} \cdot \tag{1}$$

The K ratios for *Me* and C in both phases will be equal to each other if the chemical potentials of the components in the α- and γ-phases on the interphase surface are equal.

Diffusion carbon transfer through the γ-phase to the PI is the main factor that determines the kinetics of α→γ-recrystallization during carburization.

Boundary-line concentrations were calculated using this factor. Further, the rate of advance of the interface during solid-phase diffusion changes slowly. The phase transformation was represented as a set of successive stationary states.

The scheme of a PI cell is shown in Fig. 3. The coordinate system moves with the surface. The process was considered in a two-dimensional approximation, assuming the axial symmetry of the cell. The distribution of carbon in the γ-phase ahead the flat PI in a stationary process is described by the expression:

$$^{p}X_{C}^{\gamma}(z) = {}^{\infty}X_{C}^{\alpha} + ({}^{p}X_{C}^{\gamma/\alpha} - {}^{\infty}X_{C}^{\alpha})\exp(-vz/D_{C}^{\gamma}), \tag{2}$$

where $^{\infty}X_{C}^{\alpha}$ is the mole fraction of carbon in the α-phase at an infinite distance from PI is equal to the maximum solubility, $^{p}X_{C}^{\gamma/\alpha}$ is mole fraction of carbon in the γ-phase on planar PI, v is PI advancement speed, D_{C}^{γ} is carbon diffusion coefficient in the γ-phase.
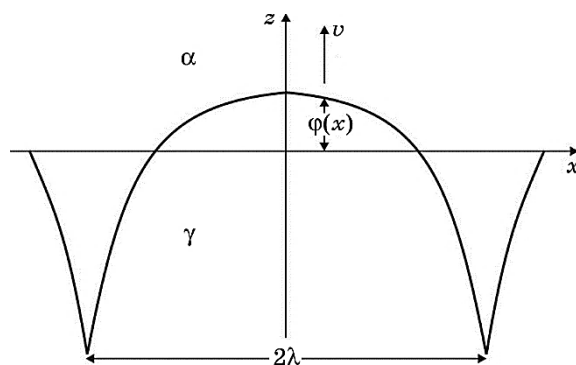
Fig. 3. Scheme of a cell at the $\alpha \to \gamma$-recrystallization front.

The mole fraction of *Me* in the γ-phase on flat PI is equal to its fraction in the initial alloy (at an infinite distance from PI), or $^{\mathrm{p}} X_{\mathrm{Me}}^{\gamma/\alpha} = ^{\infty} X_{\mathrm{Me}}^{\alpha}$. This follows from the stationarity condition. Therefore, the mole fraction of C in the γ-phase on flat PI is equal to:

$$^{\mathrm{p}} X_{\mathrm{C}}^{\gamma/\alpha} = \frac{(^{\infty} X_{\mathrm{Me}}^{\alpha} - ^{\min} X_{\mathrm{Me}}^{\gamma/\alpha})^{\max} X_{\mathrm{C}}^{\gamma/\alpha}}{^{\max} X_{\mathrm{Me}}^{\gamma/\alpha} - ^{\min} X_{\mathrm{Me}}^{\gamma/\alpha}} . \tag{3}$$

The fractions of components on the curved (cellular) PI do not correspond to the equilibrium phase diagram. This discrepancy is caused by the surface tension of the interphase boundary and, as a consequence, the appearance of capillary pressure (Laplace pressure) in one of the phases. Its value can be calculated using the formula:

$$\Delta P = \frac{2\sigma}{r}, \tag{4}$$

where σ is interfacial α/γ-tension coefficient, r is average radius of curvature of the interfacial surface.

M. Hillert's calculation [21] was used to determine the difference in the boundary concentrations between curved and flat PI. This approach was extended to a three-component system. The calculation consists of constructing a common tangent plane to the surfaces of the thermodynamic potentials G_α and G_γ for flat and curved PI. It is assumed that the concentration dependences of G_α and G_γ are known. As a result, we get the following ratio:

$$V^\gamma \Delta P^\gamma = h^{\mathrm{f}} (X_{\mathrm{C}}^{\mathrm{f}_1/\mathrm{f}_2} - ^{0} X_{\mathrm{C}}^{\mathrm{f}_1/\mathrm{f}_2}) + q^{\mathrm{f}} (X_{\mathrm{Me}}^{\mathrm{f}_1/\mathrm{f}_2} - ^{0} X_{\mathrm{Me}}^{\mathrm{f}_1/\mathrm{f}_2}), \tag{5}$$

where V^γ is molar volume of the γ-phase, ΔP^γ is pressure difference in the γ-phase on flat and curved PI,

$$\Delta P^{\gamma} = \frac{2\sigma\varphi''(x)}{\left(\left(1 + (\varphi'(x))^2\right)\right)^{3/2}},$$

σ is surface tension coefficient, ${}^0X_k^{f_1/f_2}$ is mole fraction at the interfacial surface without taking into account surface tension ($\sigma = 0$),

$$h^{f} = \left({}^0X_{C}^{\gamma/\alpha} - {}^0X_{C}^{\alpha/\gamma}\right)\frac{\partial^2 G^{f}}{\partial X_C^2}, \quad g^{f} = \left({}^0X_{Me}^{\gamma/\alpha} - {}^0X_{Me}^{\alpha/\gamma}\right)\frac{\partial^2 G^{f}}{\partial X_{Me}^2}.$$

The equilibrium mole fractions at the curved interphase boundary in both phases shift towards increasing $X_C^{f_1/f_2}$ and decreasing $X_{Me}^{f_1/f_2}$ when capillary pressure occurs in the γ-phase according to the obtained relation (5). The magnitude of the displacement depends on the magnitude of the Laplace pressure, which in turn depends on the magnitude of surface tension PI. The surface tension PI and, consequently, the capillary pressure depend on the mutual crystallographic orientation of the initial and growing phases during solid-phase recrystallization. The displacement $X_C^{\gamma/\alpha} - {}^0X_C^{\gamma/\alpha}$ will be different at different pressures in the γ-phase at the top of the cell. Thus, the geometric parameters of the cells, as well as their configuration, differ at constant values of other factors (Fig. 1, *a*, *b*).

Borderline mole fractions of components in the α- and γ-phases were calculated using relations (1), (2) and (5). The phase compositions shift along the α–γ-conduits under the influence of capillary pressure (Fig. 4). The inclination of the conode to the X_C axis is equal to $m = \left({}^0X_{Me}^{\gamma/\alpha} - {}^0X_{Me}^{\alpha/\gamma}\right) / \left({}^0X_C^{\gamma/\alpha} - {}^0X_C^{\alpha/\gamma}\right)$. We assume that the curvature of PI does not distort the concentration field X_C^{γ} due to the diffusion influx of carbon to PI determines the kinetic processes on it and is an in-
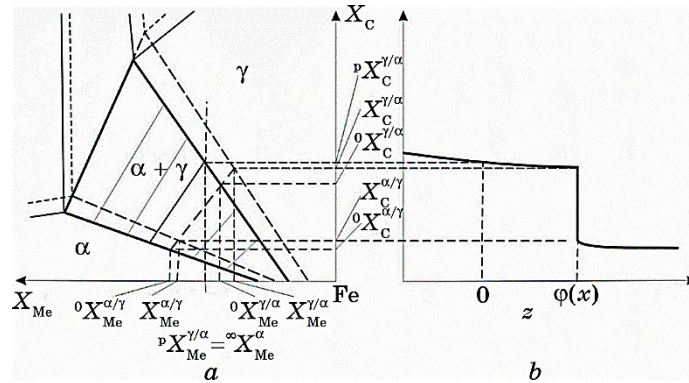
Fig. 4. Shift of equilibrium concentrations on PI: scheme of the isothermal section of the phase diagram (*a*), distribution of X_C along the depth of the carburized layer (*b*).

dependent external factor. The value $X_{\mathrm{C}}^{\gamma/\alpha}$ was calculated using formula (2). As a result, we got:

$$K = \frac{^{\infty} X_{\mathrm{C}}^{\alpha} + (^{\mathrm{p}} X_{\mathrm{C}}^{\gamma/\alpha} - {}^{\infty} X_{\mathrm{C}}^{\alpha}) \exp(-\nu\varphi(x) / D_{\mathrm{C}}^{\gamma})}{^{\max} X_{\mathrm{C}}^{\gamma/\alpha}},$$ (6)

where

$$^{\max} X_{\mathrm{C}}^{\gamma/\alpha} = {}^{\max 0} X_{\mathrm{C}}^{\gamma/\alpha} + \frac{V^{\gamma} \Delta P^{\gamma}}{(h^{\gamma} + q^{\gamma} m)^{\max 0} X}.$$

The other values of concentrations on PI were determined from relations (1):

$$\frac{X_{\mathrm{C}}^{\alpha/\gamma}}{^{\max} X_{\mathrm{C}}^{\alpha/\gamma}} = \frac{X_{\mathrm{Me}}^{\gamma/\alpha} - {}^{\min} X_{\mathrm{Me}}^{\gamma/\alpha}}{^{\max} X_{\mathrm{Me}}^{\gamma/\alpha} - {}^{\min} X_{\mathrm{Me}}^{\gamma/\alpha}} = \frac{X_{\mathrm{Me}}^{\alpha/\gamma} - {}^{\min} X_{\mathrm{Me}}^{\alpha/\lambda}}{^{\max} X_{\mathrm{Me}}^{\alpha/\gamma} - {}^{\min} X_{\mathrm{Me}}^{\alpha/\gamma}} = K,$$ (7)

where

$$^{\max} X_{\mathrm{C}}^{\alpha/\gamma} = {}^{\max 0} X_{\mathrm{C}}^{\alpha/\gamma} + \frac{V^{\gamma} \Delta P^{\gamma}}{(h^{\alpha} + q^{\alpha} m)^{\max 0} X},$$

$$^{\max} X_{\mathrm{Me}}^{\gamma/\alpha} = {}^{\max 0} X_{\mathrm{Me}}^{\gamma/\alpha} + \frac{V^{\gamma} \Delta P^{\gamma}}{(h^{\gamma} / m + q^{\gamma})^{\max 0} X}, \quad ^{\min} X_{\mathrm{Me}}^{\gamma/\alpha} = {}^{\min 0} X_{\mathrm{Me}}^{\gamma/\alpha} + \frac{V^{\gamma} \Delta P^{\gamma}}{q^{\gamma} {}^{\min 0} X},$$

$$^{\max} X_{\mathrm{Me}}^{\alpha/\gamma} = {}^{\max 0} X_{\mathrm{Me}}^{\alpha/\gamma} + \frac{V^{\gamma} \Delta P^{\gamma}}{(h^{\alpha} / m + q^{\alpha})^{\max 0} X}, \quad ^{\min} X_{\mathrm{Me}}^{\alpha/\gamma} = {}^{\min 0} X_{\mathrm{Me}}^{\alpha/\gamma} + \frac{V^{\gamma} \Delta P^{\gamma}}{q^{\alpha} {}^{\min 0} X}.$$

2.2. Mass Transfer on the Interphase Surface

The following conditions are observed during a stationary recrystallization process: the moving speed of each PI element is constant; the average content of Me in the growing γ-phase is equal to its content in the initial ferritic alloy $^{\infty} X_{\mathrm{Me}}^{\alpha}$.

The rate of advancement of PI depends on the rate of carbon supply to it through the growing γ-phase and removal into the initial α-phase. The initial α-phase has a narrow range of carbon homogeneity. Therefore, as we have already stated above, in most real cases, the mole fraction of carbon in the original ferrite is equal to its maximum solubility. Consequently, the rate of PI movement is determined only by the diffusion of carbon through the growing γ-phase. The rate of PI movement is conforming the formula:

$$\nu = -\frac{D_{\mathrm{C}}^{\gamma}}{\Delta X_{\mathrm{C}}^{\gamma-\alpha}} \frac{\partial X_{\mathrm{C}}^{\gamma}}{\partial z}\bigg|_{\varphi},$$ (8)

where $\Delta X_{\mathrm{C}}^{\gamma-\alpha} = X_{\mathrm{C}}^{\gamma/\alpha} - X_{\mathrm{C}}^{\alpha/\gamma} = X_{\mathrm{C}}^{\gamma/\alpha}(1 - {}^{\max}X_{\mathrm{C}}^{\alpha/\gamma} / {}^{\max}X_{\mathrm{C}}^{\gamma/\alpha})$.

If the boundary compositions of the phases shift along the cones under the influence of Laplace pressure, and the concentration field ${}^{\mathrm{p}}X_{\mathrm{C}}^{\gamma}(z)$ (2) is not distorted when PI is bent, then,

$$\Delta X_{\mathrm{C}}^{\gamma-\alpha} \approx X_{\mathrm{C}}^{\gamma/\alpha}(1 - {}^{\max 0}X_{\mathrm{C}}^{\alpha/\gamma} / {}^{\max 0}X_{\mathrm{C}}^{\gamma/\alpha}). \qquad (9)$$

Thus, the speed of each PI element will be the same. The PI configuration is determined by the diffusion redistribution of *Me* between phases.

The average boundary concentration of the α-stabilizer in the α-phase is higher than in the growing γ-phase. Therefore, the diffusion redistribution of a certain amount of *Me*, which was pushed into the α-phase at the initial stage of recrystallization, occurs ahead PI. This quantity is constant during a steady-state process. Diffusion processes in the α-phase ahead PI are related to the velocity ν by the following expression:

$$\nu \cos\alpha \Delta X_{\mathrm{C}}^{\gamma-\alpha} = -D_{\mathrm{Me}}^{\alpha}\left(\frac{\partial X_{\mathrm{Me}}^{\alpha}}{\partial x} + \frac{\partial X_{\mathrm{Me}}^{\alpha}}{\partial z} \right)\Bigg|_{\phi} n, \qquad (10)$$

where α is corner between the advancing direction (*z*-axis) and the normal to PI, $\cos\alpha = 1/(1 + (\partial\phi/\partial x)^2)^{1/2}$, *n* is unit vector normal to PI.

Using (1) and (7), we obtain the expression:

$$\nu \cos\alpha \left(\frac{X_{\mathrm{C}}^{\gamma/\alpha}(\Delta^{\max 0}X_{\mathrm{Me}}^{\alpha-\gamma} - \Delta^{\min 0}X_{\mathrm{Me}}^{\alpha-\gamma})}{{}^{\max 0}X_{\mathrm{C}}^{\gamma/\alpha}} + \Delta^{\min}X_{\mathrm{Me}}^{\alpha-\gamma} \right) =$$

$$= -D_{\mathrm{Me}}^{\alpha}\left(\frac{\partial X_{\mathrm{Me}}^{\alpha}}{\partial x} + \frac{\partial X_{\mathrm{Me}}^{\alpha}}{\partial z} \right)\Bigg|_{\phi} n. \qquad (11)$$

The distribution of *Me* in the γ-phase along PI was represented by a Fourier series in order for it to satisfy the stationarity condition:

$$X_{\mathrm{Me}}^{\gamma/\alpha}(x) = {}^{\infty}X_{\mathrm{Me}}^{\alpha} + \sum A_n^{\gamma/\alpha}\cos(\pi n x / \lambda), \qquad (12)$$

where $A_n^{\gamma/\alpha} = \dfrac{2}{\lambda}\displaystyle\int_0^{\lambda} dx \left(\dfrac{X_{\mathrm{C}}^{\gamma/\alpha}(x)({}^{\max}X_{\mathrm{Me}}^{\gamma/\alpha} - {}^{\min}X_{\mathrm{Me}}^{\gamma/\alpha})}{{}^{\max}X_{\mathrm{C}}^{\gamma/\alpha}} + {}^{\min 0}X_{\mathrm{Me}}^{\gamma/\alpha} + \dfrac{V^{\gamma}\Delta P^{\gamma}}{q^{\gamma}\,{}^{\min 0}x} \right)$.

$X_{\mathrm{Me}}^{\gamma/\alpha}\big|_{\varphi\,\max} < {}^{\infty}X_{\mathrm{Me}}^{\alpha}$ at the top of the cell, and *vice versa*, $X_{\mathrm{Me}}^{\gamma/\alpha}\big|_{\varphi\,\min} > {}^{\infty}X_{\mathrm{Me}}^{\alpha}$ at the base. Therefore, the diffusive transfer of *Me* occurs in the *x*-axis direction upstream of PI. The material balance during this transfer can be represented as:

$$\nu \int\limits_{0}^{\xi} dx(^{\infty}X_{\mathrm{Me}}^{\alpha} - X_{\mathrm{Me}}^{\gamma/\alpha}) = -D_{\mathrm{Me}}^{\alpha} \int\limits_{0}^{\infty} dz \left.\frac{\partial X_{\mathrm{Me}}^{\alpha}}{\partial x}\right|_{x=\xi} , \qquad (13)$$

where ξ is value x, at which $X_{\mathrm{Me}}^{\gamma/\alpha} = {}^{\infty}X_{\mathrm{Me}}^{\alpha}$.

$X_{\mathrm{Me}}^{\gamma/\alpha}$ decreases at the cell top at a constant value $X_{\mathrm{C}}^{\gamma/\alpha}$ under the influence of Laplace pressure. In case of excess pressure occurs in the α-phase and $X_{\mathrm{Me}}^{\gamma/\alpha}$ increases at the base of the cell. This creates the need to transfer more Me in a direction perpendicular to the direction of growth. However, at the same time, the average gradient $\partial X_{\mathrm{Me}}^{\alpha} / \partial x$ decreases in the α-phase, which complicates this transfer. The growth of the disturbance amplitude stabilizes according to the mechanism [20] with a more flat-topped configuration of cells at high values of σ and; therefore, higher values of ΔP^{f}. In this case, the value $X_{\mathrm{Me}}^{\gamma/\alpha}$ is close to ${}^{\mathrm{p}}X_{\mathrm{Me}}^{\gamma/\alpha}$ at the cell top, and the diffusion flux perpendicular to the growth direction at the cell top is minimized.

Longitudinal sections of the cells are shown in Fig. 5. They correspond to the limiting cases of surface tension coefficient values and microstructures in Fig. 1, *a, b*. The results of the estimated calculations $X_{\mathrm{Me}}^{\gamma/\alpha}$ are shown in Fig. 5. The disturbance amplitude $\varphi(x)$ was approximated by a piecewise continuous function during these calculations. The function consists of fragments of second-order curves and straight lines. The values of σ varied relative to the value $\sigma_{\mathrm{av}} = 10^{-2}\,\mathrm{J/m^2}$ used in Ref. [20].

As can be seen from the data presented, diffusion mass transfer in the direction of the x-axis is localized at the periphery of the cell at high values of σ. This localization brings the value $D_{\mathrm{Me}}^{\alpha} \int\limits_{0}^{\infty} dz\, \partial X_{\mathrm{Me}}^{\alpha} /x \big|_{x=\xi}$

to the value required for mass transfer.
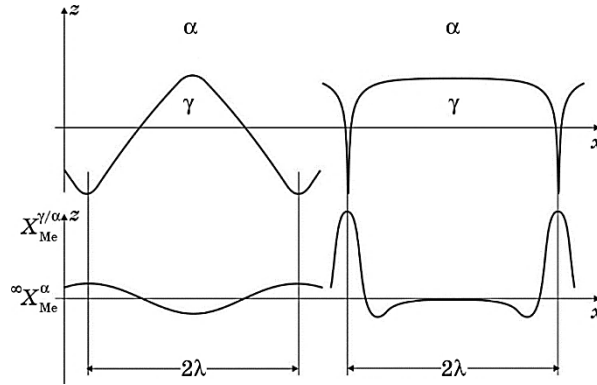
Fig. 5. PI patterns and corresponding distributions of *Me* concentrations along PI.

3. RESULTS AND DISCUSSION

PI cells have a pronounced crystalline facet upon solid-phase recrystallization. This was shown by a detailed examination of the microstructures shown in Fig. 1, *a*, *b*. The growing γ-phase has an f.c.c. lattice with a family of close-packed planes of the {111} type. They have minimal surface energy. Analysis of the traces of the faceting planes lying in the polished section showed that the octahedral {111} planes preferentially facet the PI cells.

The morphology of the cells depends on the crystallographic direction of growth of the γ phase. Usually this is one of the simple directions, coinciding with the axial structure of the carburized layer. If this direction is close to <100>, then, the shape of the cell approaches a quadrangular pyramid with a {100} plane at the base. The side faces coincide with the {111} planes of the f.c.c. lattice of the γ-phase. Thus, the angle at the cell apex changes from $\cong 70°$ (the angle between the {111} planes) to $\cong 90°$ (if the section passes through the side ribs of the <110> pyramid) in the plane of the section. The corresponding microstructure is shown in Fig. 1, *a*. The volumetric structure of cells of this type was studied in detail in Ref. [22].

The {111} plane is oriented predominantly parallel to PI in the case where the growth direction is close to <111>. Then the cell has a flat-topped morphology. Otherwise, the capillary pressure in the γ-phase at the top of the cell increases sharply. This leads to a decrease in the equilibrium concentration of *Me* at PI and the need for diffusion transfer of *Me* along the front. The lateral surfaces of the cells are also faceted by {111} planes, and the cells are an inclined prism (Fig. 1, *b*).

Two or more columnar crystals of the γ-phase can grow from one grain of the α-phase. Therefore, the crystal lattices of the initial α- and growing γ-phases are randomly oriented relative to each other. The {110} set of planes are the planes of lowest energy in the b.c.c. lattice of the initial α-phase. If one of the {111} faceting planes of the growing γ-phase turns out to be parallel to the {110} α-phase, the total PI energy decreases sharply. At the same time, the growth rate of this face increases. If {111} γ and {110} α are mutually oriented according to one of the variants of the Kurdjumov−Sachs orientation relation, for example, $(111)\gamma \parallel (011)\alpha$, $[10\bar{1}]\gamma \parallel [1\bar{1}1]\alpha$; then, the growth of the faceting plane occurs at maximum speed. An increase in the growth rate of one of the boundary planes leads to the fact that the PI structure becomes similar to Widmanstätten one.

4. CONCLUSION

Studies of steady-state α→γ-recrystallization during isothermal carburization of a ferritic iron alloy with a cellular structure of the inter-

phase boundary have been carried out.

Diffusion transfer of carbon through the γ-phase to the interphase surface is the main factor that determines the kinetics of $\alpha \rightarrow \gamma$-recrystallization during carburization.

The $\alpha \rightarrow \gamma$-phase transformation was represented as a set of successive stationary states. The $\alpha \rightarrow \gamma$-transformation process was considered in a two-dimensional approximation, assuming axial symmetry of the cell. An expression for the distribution of carbon in the γ-phase upstream of the flat PI during a steady-state process was derived.

The mole fractions of components on cellular PI do not correspond to the equilibrium phase diagram due to the surface tension of the α/γ-interface and, as a consequence, the appearance of capillary pressure in one of the phases.

The boundary concentration differences between curved and flat PI were determined by constructing a common tangent plane to the surfaces of thermodynamic potentials G_α and G_γ for flat and curved PI.

The boundary mole fractions of the components in the α- and γ-phases were calculated. It was assumed that the phase compositions shift along the $\alpha-\gamma$-conduits under the influence of capillary pressure.

Diffusion processes in the α-phase before PI have been described. The average boundary concentration of the α-stabilizer in the α-phase is higher than in the growing γ-phase. An expression connecting diffusion processes in the α-phase before PI with the speed of front advancement was obtained.

Longitudinal sections of cells corresponding to limiting cases of surface tension coefficient σ and microstructures during $\alpha \rightarrow \gamma$-recrystallization are presented. The disturbance amplitude $\varphi(x)$ was approximated by a piecewise continuous function consisting of fragments of second-order curves and straight lines when performing these calculations.

A detailed study of the microstructures of the transformation front shows that PI cells have a pronounced crystalline facet during solid-phase recrystallization. The growing γ-phase has an f.c.c. lattice with a set of close-packed planes of the {111} type, which have minimal surface energy. The morphology of the cells depends on the crystallographic direction of growth of the γ-phase. Usually, this is one of the simple directions, coinciding with the axial structure of the carburized layer.

Two or more columnar crystals of the γ-phase can grow from one grain of the α-phase. The growth of the boundary plane occurs at the maximum speed if {111} γ and {110} α are mutually oriented according to one of the variants of the Kurdjumov–Sachs orientation relationship.

The resulting model can be used as a base model for studying the growth of a natural austenite–carbide composite.

REFERENCES

1. R. D. Sisson, J. R. Dayananda, and M. A. Dayananda, *Metal. Trans.*, **3**: 647 (1972).
2. O. V. Movchan and K. O. Chornoivanenko, *Usp. Fiz. Met.*, **19**, No. 2: 185 (2018).
3. W. W. Mullins and R. F. Sekerka, *J. Appl. Phys.*, **35**: 444 (1964).
4. R. F. Sekerka, *J. Appl. Phys.*, **36**: 264 (1965).
5. S. R. Coriell and R. F. Sekerka, *Rapid Solidification Processing: Principles and Technologies* (Eds. R. Mehrabian, B. H. Kear, and M. Cohen) (Louisiana: Claitor's, Baton Rouge: 1980), p. 35.
6. S. R. Coriell, G. B. McFadden, and R. F. Sekerka, *Ann. Rev. Mater. Sci.*, **15**: 119 (1985).
7. S. R. Coriell and G. B. McFadden, *Handbook of Crystal Growth* (Ed. D. T. J. Hurl) (Amsterdam: Elsevier, 1993), vol. 1a, p. 785.
8. S. H. Davis, *Theory of Solidification* (Cambridge: Cambridge University Press: 2001).
9. K. P. Bunin, V. Y. Movchan, and V. V. Nikiforova, *Izvestiya VUZov. Chernaya Metallurgiya*, **2**: 106 (1977) (in Russian).
10. V. Y. Movchan and V. V. Vladimirova, *Izvestiya AN SSSR. Metally*, **6**: 52 (1988) (in Russian).
11. K. P. Bunin, V. I. Movchan, and L. G. Pedan, *Izvestiya VUZov. Chernaya Metallurgiya*, **2**: 123 (1973) (in Russian).
12. K. P. Bunin, V. I. Movchan, and L. G. Pedan, *Izvestiya AN SSSR. Metally*, **3**: 164 (1975) (in Russian).
13. V. I. Movchan, L. G. Pedan, and V. P. Gerasimenko, *MiTOM*, No. 9: 19 (1983) (in Russian).
14. V. I. Movchan, L. G. Pedan, and V. I. Ivanitsa, *MiTOM*, No. 8: 12 (1990) (in Russian).
15. V. M. Gavrilenko, V. P. Gerasimenko, and V. I. Movchan, *Izvestiya AN SSSR. Metally*, **3**: 71 (1984) (in Russian).
16. A. V. Movchan, S. I. Gubenko, A. P. Bachurin, and E. A. Chernoivanenko, *Stroitel'stvo, Materialovedenie, Mashinostroenie*, **64**: 262 (2012) (in Russian).
17. O. V. Movchan and K. O. Chornoivanenko, *Metallurgical and Ore Mining Industry*, **5−6**: 76 (2019) (in Ukrainian).
18. K. P. Bunin, V. Y. Movchan, and V. V. Nikiforova, *Izvestiya VUZov. Chernaya Metallurgiya*, **10**: 121 (1974) (in Russian).
19. K. P. Bunin, V. Y. Movchan, and V. V. Nikiforova, *Izvestiya VUZov. Chernaya Metallurgiya*, **10**: 103 (1976) (in Russian).
20. O. V. Movchan and K. O. Chornoivanenko, *Metallofiz. Noveishie Tekhnol.*, **41**, No. 1: 13 (2019).
21. M. Hillert, *Phase Equilibria, Phase Diagrams and Phase Transformations* (Cambridge: Cambridge University Press: 2007).
22. V. Y. Movchan, V. P. Gerasimenko, and T. N. Odynchenko, *Izvestiya AN SSSR. Metally*, **4**: 116 (1981).